Stanford Exploration Project, Report 94, November 11, 1997, pages 17–32

Stanford Exploration Project, Report 94, November 11, 1997, pages 17–32

Detecting S-wave velocity contrasts across BSRs using AVO

Christine Ecker[1]

keywords: *AVO, S-wave velocity, hydrate*

ABSTRACT

Reservoir characterization of methane hydrate data requires a reasonable estimate of their S-wave velocity behavior. AVO analysis at the bottom simulating reflector (BSR), which is the reflection off the bottom of a stable hydrate structure, is a tool to extract this information from surface P-wave data. Using sonic and density logging data from a recent ODP (Ocean Drilling Program) cruise at the Blake Outer Ridge, offshore Florida and Georgia, I evaluate the effect of different S-wave velocity structures on the seismic BSR amplitudes by forward seismic modeling. I show that even for an angle coverage of 30 degrees, S-wave velocity contrasts of about ± 17 m/s across the BSR can still be uniquely distinguished in the case of ideal amplitudes. Introduction of random Gaussian noise of a S/N ratio of about 2:1 strongly reduces the ability to differentiate between such small contrasts. In that case, errors between ± 50 m/s and ± 100 m/s can be introduced into the estimation of the shear wave velocity contrast. A subsequent 2-D inversion of a model, that varies laterally only in S-wave velocity, results in a more stable resolution in the presence of noise.

INTRODUCTION

The reservoir characterization of methane hydrate structures plays an important role in evaluating the potential of hydrate fields as future energy reserves. Key parameters that are of interest are the amount of hydrate present, its mobility and recoverability. Increasingly, these are attempted to be inferred from drilling (MacKay et al., 1994; Matsumoto et al., 1996). However, the risk of heating and destabilizing the initial hydrate conditions is considerably high. Thus, core-samples and well-log data do not necessarily reflect the correct in-situ hydrate conditions. Consequently, it is important to infer elastic and mechanical properties from surface seismic data (Laberg and Andreassen, 1996; Brown et al., 1996; Ecker et al., 1996; Ecker and Lumley, 1994; Yuan et al., 1996) or VSP (Holbrook et al., 1996). Most of these investigations were

[1]**email:** christin@sep.stanford.edu

based mainly on AVO responses and synthetic modeling using P-wave velocity information, accessible directly from the seismic data, and neglected possible important S-wave velocity effects entirely. However, as Ecker et al. (1996) have shown, different S-wave velocity behavior might have significant impacts on the hydrate properties, thus influencing assessments of the amount of hydrate, its position in the pore space and its effect on the surrounding sediment strength.

The recent ODP (Ocean Drilling Program) drilling cruise at the Blake Bahama Ridge and Carolina Rise implemented for the first time a dipole shear wave tool in in-situ hydrates structures (Matsumoto et al., 1996). This might give some first order insight in the S-wave velocity behavior of methane hydrates. However, since hydrate is considerably unstable for already small changes in pressure and temperature conditions, the process of drilling might have perturbed the actual in-situ properties. Therefore, it will be important to tie the well information to information obtained from surface seismic which does not influence the hydrate properties. But how good can S-wave velocity behavior be estimated from marine P-wave data?

AVO analysis and inversion is a common tool for attempting to extract S-wave velocity information from seismic data (Ostrander, 1984; Spratt et al., 1993). The precision of the result and its resolution, however, strongly depends on the angle coverage of the data, data quality, noise contamination and data processing (Swan, 1993; Tura and Hanitzsch, 1995; van Wijngaarden and Berkhout, 1996). Considering these effects, what kind of S-wave velocity contrasts can be resolved from surface seismic with regard to the transition from hydrated to non-hydrated sediment? How small can they be and still be distinguishable?

In this paper, I evaluate the effect of different S-wave velocity contrasts at the bottom simulating reflector (BSR) on seismic amplitudes. The BSR is the reflection off the base of the hydrate stability field, thus marking the transition from hydrated to non-hydrated sediment. I use P-wave sonic log and density data from one of the wells drilled during the ODP drilling cruise at the Blake Outer Ridge to obtain a blocked velocity and density model. An S-wave velocity model was obtained by fitting an approximate linear trend to preliminary published shear dipole data (Matsumoto et al., 1996). Changing the S-wave velocity behavior at the BSR reflection, I forward model different seismic scenarios that resemble different S-wave velocity contrasts across the BSR. AVO analysis of single modeled CMP gathers data shows that even very small S-wave velocity contrast of about $\pm$ 17 m/s can still be uniquely distinguished in their amplitude behavior. Subsequently, I simulate a more realistic data environment by adding random Gaussian noise with a S/N ratio of 2:1. This introduces significant variations in the seismic amplitude responses, and thus causes the AVO trend of the different models to overlap. The unique resolution of the models depends strongly on the standard deviation of the data. Even a qualitative analysis to enable the determination of the sign of the contrast (positive or negative) can be quite hard. Assuming small lateral changes in the subsurface structure, averaging of neighboring CMP gathers should, however, improve this analysis. A subsequent 2-D seismic migration/inversion of a velocity model varying laterally only in S-wave velocity shows that even in the presence of noise a reasonable good result can be obtained.

AVO THEORY

AVO is a common tool for extracting shear wave information from P-wave seismic data (Ostrander, 1984). For plane waves, the PP reflection coefficient is given by Zoeppritz equations which give a relation between velocity and density layer contrasts in dependence of the angle of incidence. A linearized form of $R_p(\theta)$ was derived by Aki and Richards (Aki and Richards, 1980):

$$R(\theta) = c_1(\theta)\, I_p + c_2(\theta)\, I_s + c_3(\theta)\, D$$

with

$$c_1(\theta) = \frac{1}{2\cos^2(\theta)},$$

$$c_2(\theta) = -4\,\gamma^2 \sin(\theta)^2, \text{ and}$$

$$c_3(\theta) = 2\gamma^2 \sin^2(\theta) - \tfrac{1}{2}\tan^2(\theta)$$

The P-impedance contrast is denoted by I_p, the S-impedance contrast by I_S and the density contrast by D. P-impedance and S-impedance contrast are functions of either P- or S-wave velocity contrast and density contrast. θ is the angle of incidence and γ denotes the background v_s/v_p ratio. For small angles, only $c_1(\theta)$ contributes to the reflection coefficient, meaning that at near zero-offset it is dominated by the P-impedance contrast. For larger angles, the coefficient $c_2(\theta)$ also starts to affect the amplitudes, thus introducing shear wave velocity information into the data. The density contrast will only be included in the amplitude information for very large angles, thus will be neglected in this study.

Based on the analytic form of the reflection coefficient, it can be interpreted as having all the acoustic information in the near-zero offsets and additional shear impedance information in the far offsets. The longer the offsets, that is the higher the angles, the more $c_2(\theta)$ will contribute to the amplitudes and the more the amplitude will be sensitive to changes in the shear properties across layers. If the angle coverage is only medium (i.e. up to 30-35 degrees), the amplitude will be significantly more sensitive to acoustic changes. This means that in case of large amplitude variations i.e. due to noise, the shear impedance contrast will be less well constrained than the acoustic impedance contrast.

DATA

I use sonic and density logging data from the ODP drilling cruise at the Blake Outer Ridge (Matsumoto et al., 1996) to evaluate the effect of different S-wave velocity contrasts at the transition from hydrate to non-hydrate bearing sediment. Since the drilling was performed in the vicinity of multi-channel surface seismic data that were provided to me by the USGS (Ecker and Lumley, 1994; Ecker et al., 1996), the drilling results will provide some further insight into the possible interpretation of the seismic data.

The fine layered sonic and density logs were upscaled to about 5 m in depth to be comparable with the seismic wavelength scale. For the upscaling, I used an equivalent medium averaging approach (Muir et al., 1992; Lumley et al., 1994). Since the dipole shear data are not yet publically available, I estimated an approximately linear trend to the preliminary published shear data and extrapolated it to the seafloor. As this study requires the changing of the S-wave velocities across the BSR, I blocked the data in order to create a better control over the velocity substitution. The blocking was done by averaging the data within layers of variable thickness. The upscaled and subsequently blocked data can be seen in Figure 1.

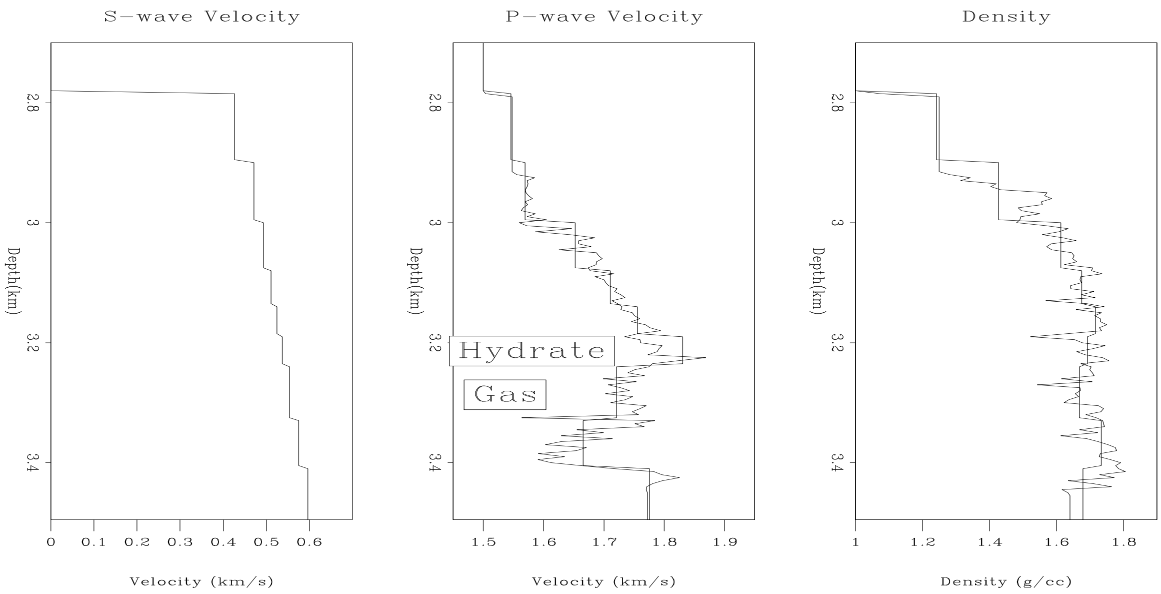

Figure 1: The left panel shows a blocked approximation to the shear wave log. The middle and right panel show the upscaled acoustic and density log and the subsequent blocked model. christin1-wells-block-ann [ER]

The well data show an increase in acoustic velocity in the hydrated sediments and a decrease in the underlying sediments which are gas saturated. This is in good agreement with surface seismic observations in the area (Wood et al., 1994; Katzman et al., 1994; Ecker and Lumley, 1994). Furthermore, there is a small decrease in density at the BSR due to the fact that the hydrate density is higher than the gas density. The approximated shear wave data show overall a very low S-wave velocity trend. The drilling showed that the sediments in this area are highly unconsolidated (porosity more than 50%) and contain a significant amount of clay. Thus, Poisson's ratios of more than 0.4 does not seem surprising.

1-D MODELING

The blocked data described in the previous section are used to evaluate the effect of different shear velocity contrasts across the BSR on seismic amplitudes. To do so, I vary the contrast at the transition from hydrate bearing sediments to the underlying gas sediments. In this way, I simulate either a positive shear wave velocity contrast or a negative shear wave velocity contrast (Figure 2). A positive contrast is characterized by an increase of the shear wave velocity at the transition from hydrate to gas, while a negative contrast means that Vs decreases across the BSR.

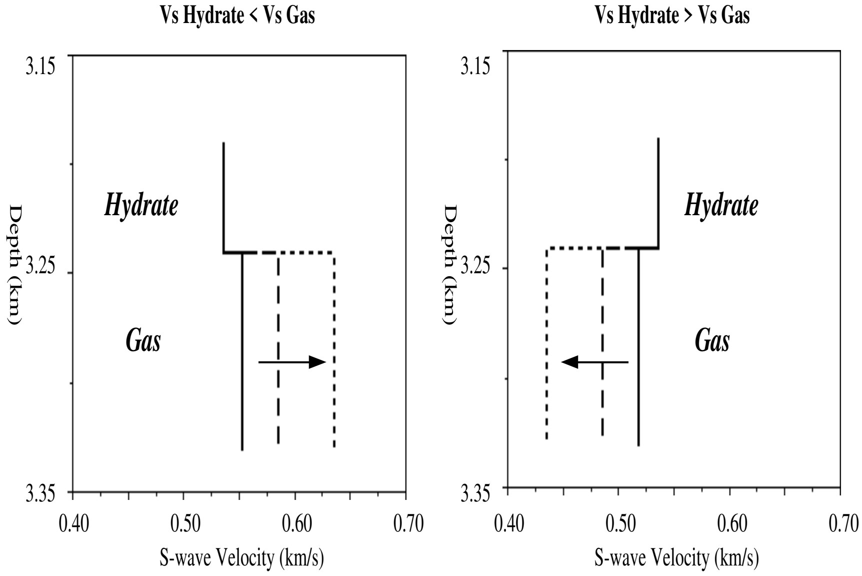

Figure 2: S-wave velocity contrast variations across the BSR. The left panels shows an increase in the shear contrast (+), while the right one shows a decrease in shear contrast (-). The contrasts vary from ± 17 m, ± 50 m to as much as ± 100 m. christin1-contrasts [NR]

The forward modeling was performed by generating synthetic seismograms using a generalized Kirchhoff body force scattering theory by Lumley and Beydoun (Lumley and Beydoun, 1993). This technique combines Zoeppritz plane-wave reflection and Rayleigh-Sommerfeld elastic diffraction responses and generates correct AVO responses for locally planar reflectors. The method computes only primary reflections, which is, however, sufficient for this case. Due to the very thick water layer of nearly 3 km, seismic data do not show multiple contamination or converted shear waves. I used the blocked elastic parameters described before as input into the modeling code and generated CMP gathers with different shear contrasts across the BSR. The P-wave velocities and densities were kept constant. Each CMP gather has a near-offset of 0.3 km and a far offset of 3.9 km. The offset spacing is 50m. This simulates the typical surface seismic aquisition scheme used to acquire data in the Blake Ridge region.

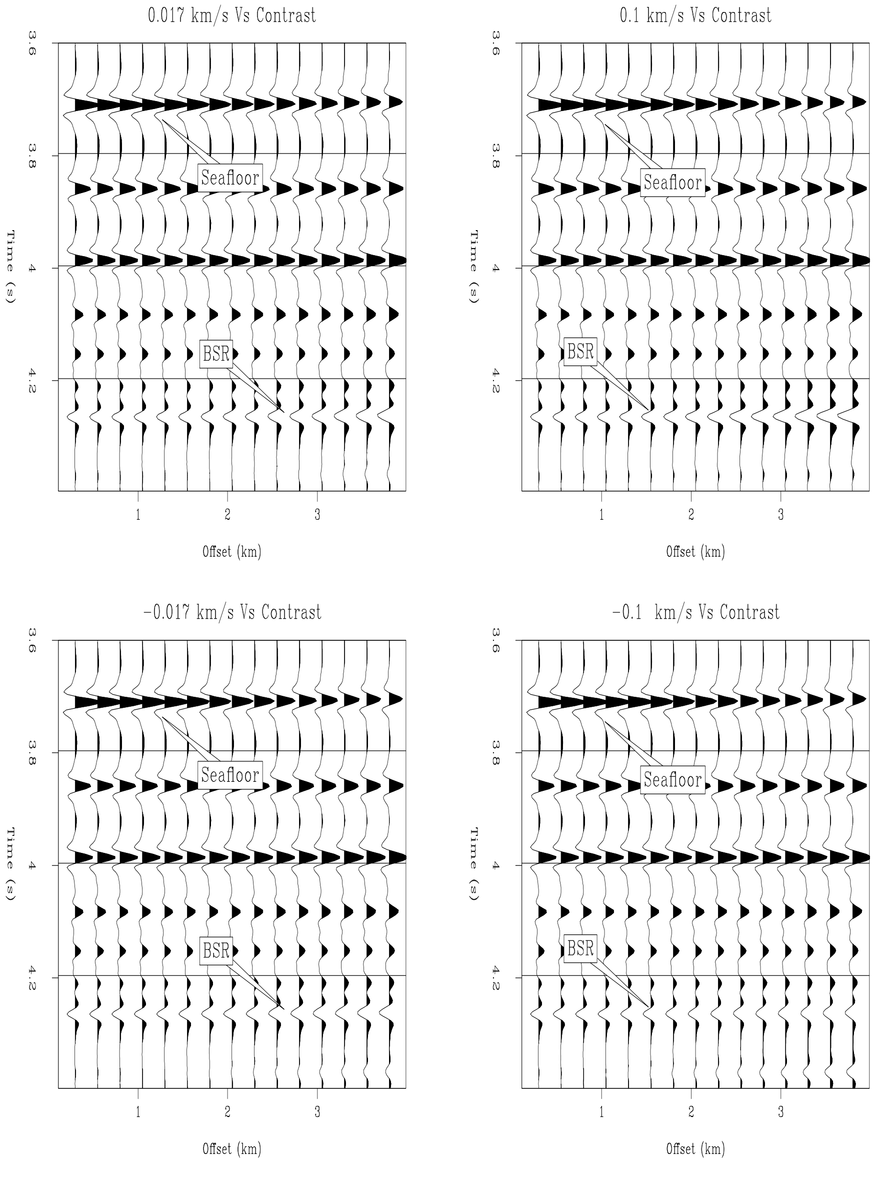

Figure 3: Synthetic CMP gathers for S-wave velocity contrasts of ± 17 m/s and ± 100 m/s. christin1-vs-ann [CR]

Figure 3 shows the modeling result after applying spherical divergence correction and NMO correction. The upper two CMP gathers were obtained by assuming a positive shear contrast at the BSR, the lower ones were generated with a negative contrast. The contrasts varied from being very small (± 17 m/s) to being about ± 100 m/s. The synthetic gathers show that the positive contrast is characterized by an increase in the BSR amplitude with increasing offset. The negative contrasts display the reverse behavior. To emphasize the different amplitude behavior, I picked the amplitudes in each CMP gather along the BSR reflection at approximately 4.29s two-way traveltime. The picked amplitudes can be seen in Figure 4.

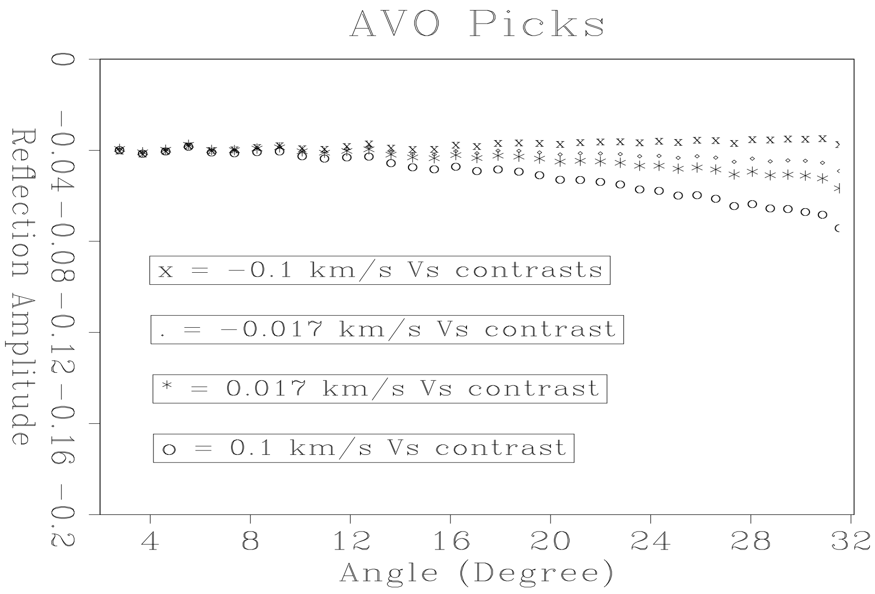

Figure 4: Picked BSR amplitudes versus angle. christin1-avo-ann [ER]

The picked AVO curves can be uniquely distinguished at large angles even in case of very small shear contrasts. Since the P-wave velocities and densities did not change during the modeling, the curves are in agreement for small angles. They start to differ at larger angles due to the changing shear wave velocity contrasts. Least-squares inversion using the linearized Zoeppritz equation will result in well constrained P- and S-impedance contrasts.

Real data, on the other hand, never display such a clean amplitude behavior. Amplitudes are affected by different phenomena such as transmission, array attenuation, spherical divergence, multiples, random noise and so on. Processing to recover the true amplitude unperturbed by those effects has the danger of not correcting for all occurring amplitude losses or not preserving the amplitude information. This will lead to errors in the amplitudes that can not be easily quantified anymore. In the case of ideal processing and correcting, the data will still be contaminated by random noise which will influence the amplitudes.

In order to simulate a more realistic data setting, I added random Gaussian noise to my data. The magnitude of the noise was approximately half that of the near offset

BSR amplitude. The resulting noisy CMP gathers can be seen in Figure 5. The data display quite a variance in their amplitudes and obvious distortions.

Figure 5: Synthetic, noisy CMP gathers for S-wave velocity contrasts of ± 17 m/s and ± 100 m/s. christin1-vs-noise-ann [CR]

For the detection of the elastic layer properties from the BSR AVO behavior, it is important to know how long these amplitudes can still be uniquely distinguished using AVO analysis. This concerns the far offsets in particular since they carry all the S-wave velocity information. Using the known standard deviation of the data, it is possible to put error bars around the noise free amplitude and predict the variance of the noisy data and thus the possible resolution of two different AVO events. Figure 6 shows the true amplitude picks for data with the corresponding error bars. The error bars give a 95% confidence interval for the deviation of the noisy data from the true data at a certain angle. Amplitude picks from two different CMP gathers can only be resolved in their curvature when the difference between the true values is larger than the error bar. Since the AVO curves will agree at small angles due to the same P-wave velocity and density contrast, Figure 6 focuses on angles above 25 degrees.

The left panel of figure 6 shows the comparison of amplitudes associated with ± 17 m/s shear contrast across the BSR. It is obvious that these two events will not be resolvable once the noise is added to the data. The middle panel shows a comparison between amplitudes caused by ± 50 m/s Vs-contrasts. In this case, the two events might barely be distinguished. For ± 100 m/s contrasts, however, there appears to be a clear resolution between the data at large angles.

Figure 7 displays the actual picked BSR amplitudes from the synthetic, noisy CMP gathers. As predicted from the error bars, the picks from ± 17 m/s Vs-contrasts cannot be distinguished anymore. The data also shows a lot of overlapping for the case of ± 50 m/s shear velocity contrasts. However, as the prediction has shown, these might be just resolvable. It is obvious, however, that the picks of the 100 m/s and -100 m/s contrasts are distinguishable.

In the case of a least-squares inversion of these data for the layer properties, this means that there would be at least an error of ± 50 m/s on an observed shear contrast, if not more. In the case of small contrasts, even the sign of the S-wave velocity contrast (positive or negative) cannot be uniquely inferred anymore. The error will of course vary with the amount of deviation in the amplitude. As mentioned before, the P-wave velocity contrast is much more stable even for such data variance and will be better constrained.

In order to improve the data quality and to reduce the random noise, one could assume that the lateral layer properties do not change significantly over a certain region. In that case, the averaging of the amplitudes of several CMPs will give an improved AVO response. However, also in this case the small shear contrasts and thus the important uniqueness of the sign of the contrast might be lost.

2-D MODELING

In this section, I explore the effect of a full 2-D inversion for P- and S-impedance contrasts as opposed to the local observation of AVO amplitudes. I constructed a 2-D model consisting of the blocked sonic velocities and densities. They were kept laterally constant. The S-wave velocity model does have laterally changing S-wave velocities across the BSR. These variations have the same magnitudes as in the previous section. The sonic and shear velocities are displayed in Figure 8.

After generating CMP gathers every 50 m along the 2-D model, I performed a true amplitude migration in order to collapse the diffractions caused by the laterally varying S-wave velocity contrasts. Subsequently, I applied a least-squares impedance inversion (Lumley and Beydoun, 1993). This technique fits the prestack migrated

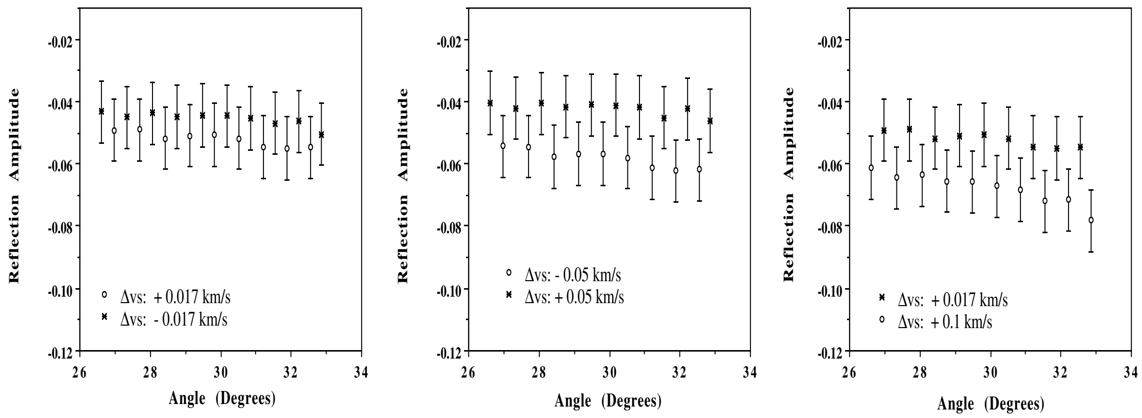

Figure 6: Noise-free amplitudes and their error bars for the expected standard deviation. christin1-errors2 [NR]

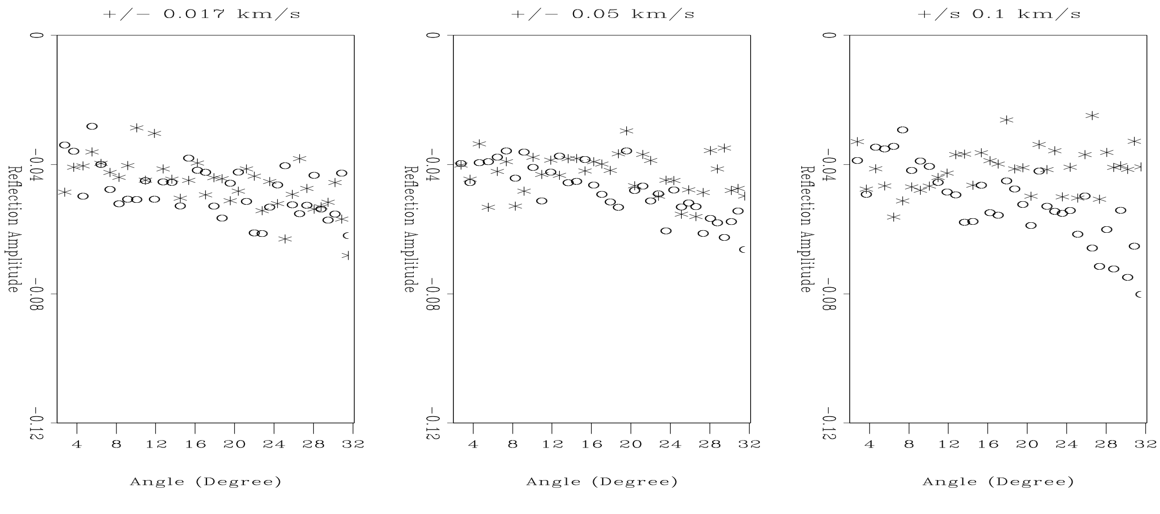

Figure 7: Amplitude picks from synthetic CMP gathers for ±17 m/s, ±50 m/s, and ±100 m/s S-wave velocity contrasts across the BSR. christin1-avo-noise [ER]

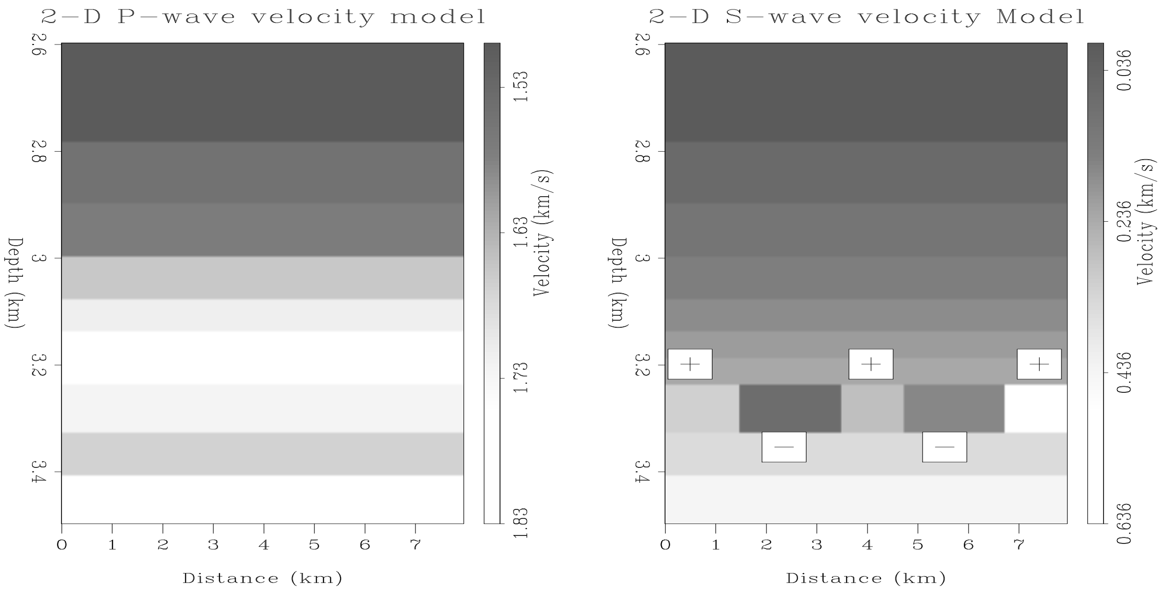

Figure 8: P-wave and S-wave interval velocity models. christin1-model-ann [CR]

AVO gathers at each pseudo-depth and surface position to the theoretical P- and S-impedance curves based on the linearized Zoeppritz equations. The study was performed both for noise free and noisy data.

Figure 9 shows the noise free P- and S-impedance contrast sections zoomed in around the BSR. It shows a strong negative P-impedance contrast (black), and the variations from positive to negative S-wave impedance contrasts. The result based on noisy data is shown in Figure 10. The signal to noise ratio was again approximately 2:1 for the BSR amplitudes. As expected, the P-wave impedance looks very similar to the previous one. The S-wave impedance, on the other hand, appears much noisier than before. It is harder to differentiate between the small positive and negative contrasts between 4 and 6 km distance. Since the P-impedance contrast is uniform through the section, a P*S impedance map should emphasize areas where the P-and S-impedance are either both negative/positive or have different sign. This will give some insight into the qualitative behavior of the shear wave velocity from hydrate to the underlaying sediments. The result can be seen in Figure 11.

Although the data is contaminated by noise, the P*S impedance contrast map shows the areas of negative S-wave velocity contrasts (white) and positive S-wave velocity contrast (black). Even the small contrasts are visible in the map. Though the amplitudes of the data can not be distinguished using a 1-D local AVO analysis, the 2-D inversion and subsequent properly chosen attribute map results in a higher resolution. When picking the amplitudes along a reflector, one usually picks the maximum positive or negative peaks. These may, however, not always line up perfectly after NMO correction. Thus, when fitting the theoretical impedance curves to each pseudo-depth surface position, which is done along a straight line, the 2-D inversion already somewhat averages out some of the noise.

CONCLUSION

I evaluated the effect of different S-wave velocity contrasts at the BSR on seismic amplitudes by modeling synthetic CMP gather for different shear wave velocity contrasts. Increasing velocities display a pronounced increase of amplitudes with offset. Negative velocity contrasts show either near to constant AVO behavior or a slight decrease in amplitude with offset. This depends on the magnitude of the contrast itself. AVO analysis of these single modeled CMP gathers showed that even very small S-wave velocity contrasts of only $\pm$ 17 m/s can be distinguished in the case of ideal amplitudes. Simulating more realistic data by adding a random Gaussian noise to the data introduces significant variances in the seismic amplitudes. The resolution of the different models depends strongly on the data variance, and even a qualitative analysis to determine the sign of the Vs contrast (positive or negative) can be impossible. A subsequent 2-D seismic migration/inversion of a 2-D model suggests that even in the presence of noise, a reasonably good result can be obtained.

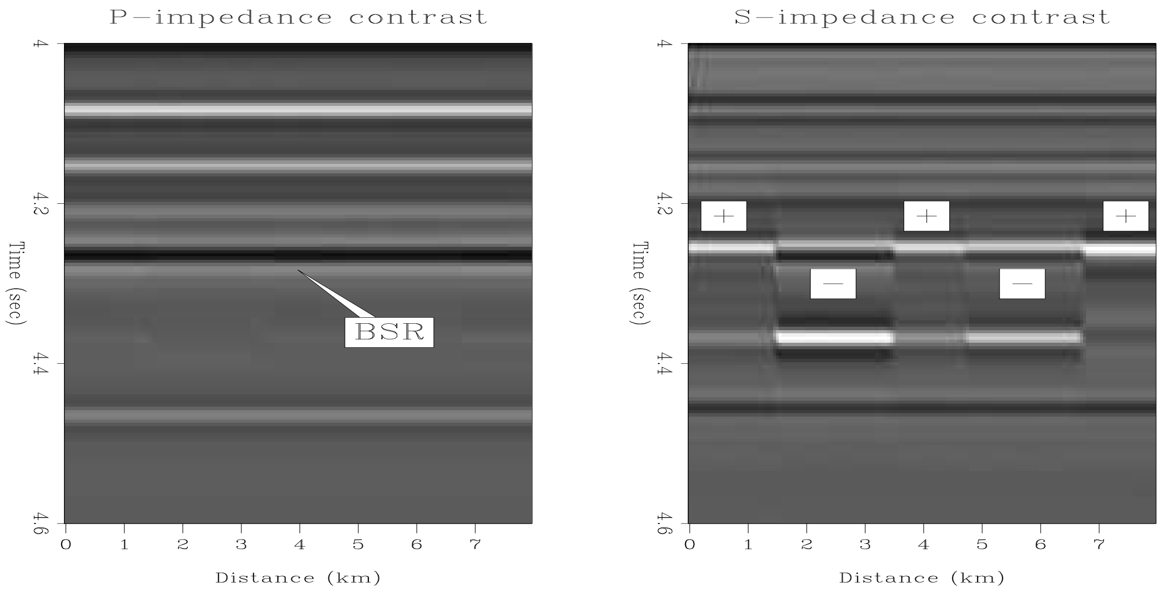

Figure 9: P-impedance and S-impedance contrasts for noise-free data. christin1-imped-ann [CR]

ACKNOWLEDGMENTS

I would like to thank Tim Collett from the USGS in Denver and Jack Dvorkin from the Stanford Rock Physics Group for providing me with the well data.

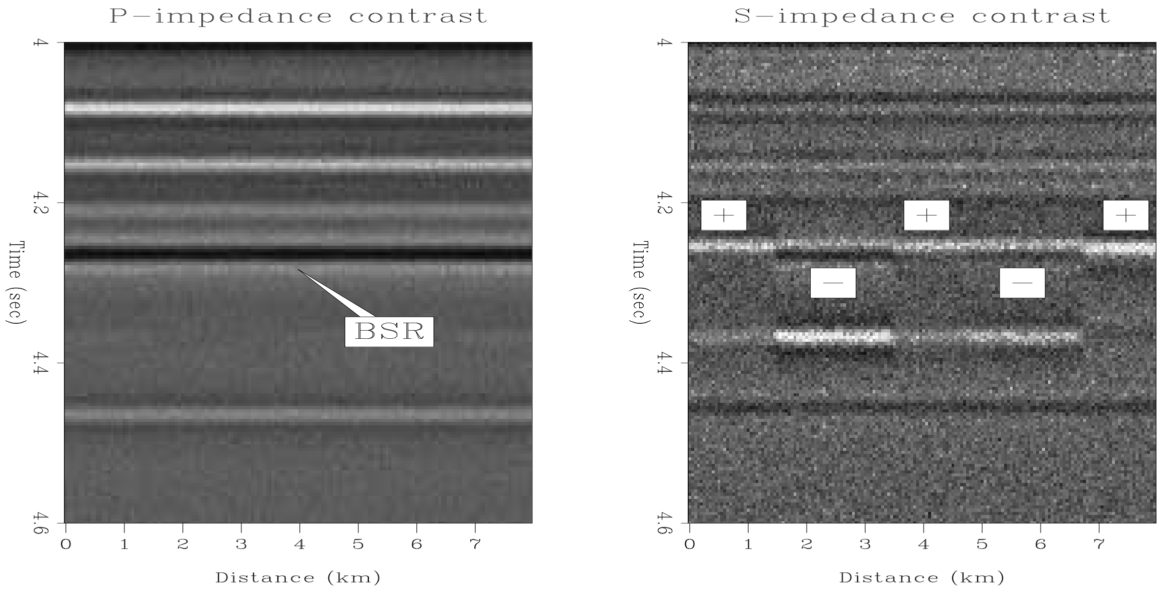

Figure 10: P-impedance and S-impedance contrasts for noisy data. christin1-imped-noise-ann [CR]

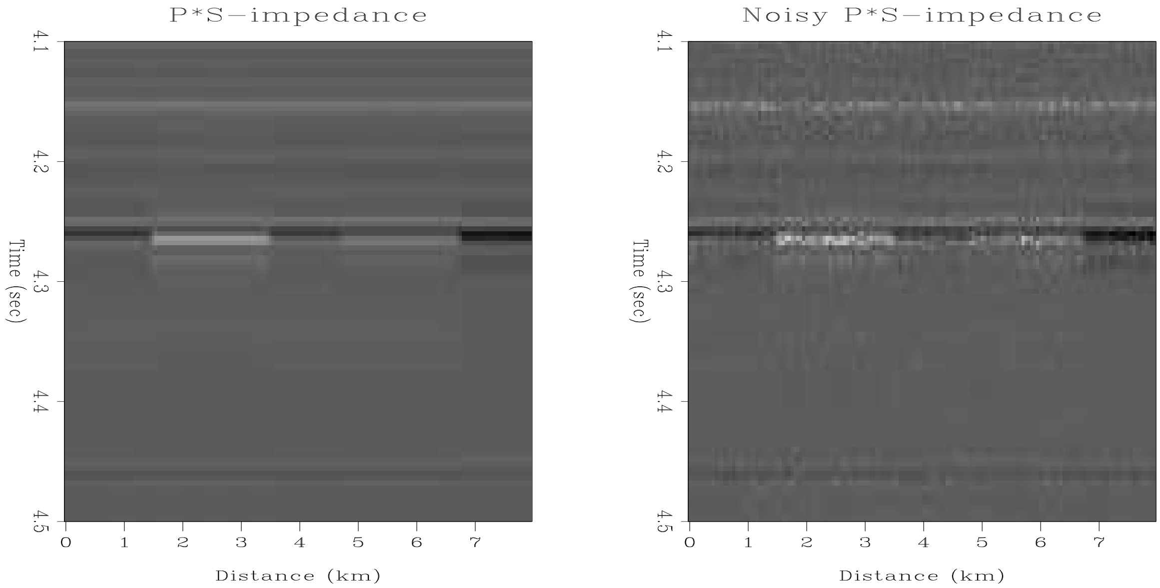

Figure 11: P*S impedance contrast maps for noise-free data (right panel) and noisy data (right panel). christin1-psmap [CR]

REFERENCES

Aki, K., and Richards, P. G., 1980, Quantitative seismology: Theory and methods: W. H. Freeman and Co., New York.

Brown, K. M., Bangs, N. L., Froelich, P. N., and Kvenvolden, K. A., 1996, The nature, distribution, and origin of gas hydrate in the Chile Triple Junction region: Earth and Planet. Sci. Lts., **139**, 471–483.

Ecker, C., and Lumley, D. E., 1994, Seismic AVO analysis of methane hydrate structures: 64th Ann. Internat. Meeting, Soc. Expl. Geophys., Expanded Abstracts, 1100–1103.

Ecker, C., Dvorkin, J., and Nur, A., 1996, Sediments with gas hydrates: Internal structure from seismic AVO: Geophysics, submitted for publication.

Holbrook, W. S., Hoskins, H., Wood, W. T., Stephen, R. A., Lizarralde, D., and the Leg 164 Scientific Party, 1996, Methane hydrate and free gas on the Blake Ridge from vertical seismic profiling: Science, **273**, 1840–1843.

Katzman, R., Holbrook, W. S., and Paul, C. K., 1994, Combined vertical-incidence and wide-angle seismic study of a gas hydrate zone, Blake Ridge: J. Geophys. Res., **99**, 17975–17995.

Laberg, J. S., and Andreassen, K., 1996, Gas hydrate and free gas indications within the Cenozoic succession of the Bjornoya Basin, western Barents sea: Marine and Pet. Geol., **13**, 921–940.

Lumley, D. E., and Beydoun, W. B., 1993, Angle-dependent reflectivity estimation by Kirchhoff migration/inversion: Theory: SEP–**79**, 205–226.

Lumley, D. E., Nur, A., Strandenes, S., Dvorkin, J., and Packwood, J., 1994, Seismic monitoring of oil production: A feasibility study: 64th Ann. Internat. Meeting, Soc. Expl. Geophys., Expanded Abstracts, 319–322.

MacKay, M. E., Jarrard, R. D., Westbrook, G. K., and Hyndman, R. D., 1994, Origin of bottom-simulating reflectors : Geophysical evidence from the Cascadian accretionary prism: Geology, **22**, 459–462.

Matsumoto, R., Paull, C., Wallace, P., and the Leg 164 Scientific party, 1996, Gas hydrate sampling on the Blake Ridge and Carolina Rise: ODP, Leg 164 Preliminary Report.

Muir, F., Dellinger, J., Etgen, J., and Nichols, D., 1992, Modeling elastic fields across irregular boundaries: Geophysics, **9**, 1189–1193.

Ostrander, W. J., 1984, Plane-wave reflection coefficients for gas sands at nonnormal angles of incidence: Geophysics, **49**, 1637–1649.

Spratt, R. S., Goins, N. R., and Fitch, T. J., 1993, Pseudo-shear - The analysis of AVO *in* Castagna, J. P., and Backus, M. M., Eds., Offset dependent reflectivity - Theory and practice of AVO analysis:: Soc. Expl. Geophys., 37–56.

Swan, H. W., 1993, Properties of direct AVO hydrocarbon indicators *in* Castagna, J. P., and Backus, M. M., Eds., Offset dependent reflectivity - Theory and practice of AVO analysis:: Soc. Expl. Geophys., 78–92.

Tura, M. A. C., and Hanitzsch, C., 1995, Influence of velocity uncertainty on avo migration/inversion: 65th Ann. Internat. Mtg., Soc. Expl. Geophys., Expanded Abstracts, 1028–1031.

van Wijngaarden, A. J., and Berkhout, A. J., 1996, Resolution analysis and AVO attributes: 66th Ann. Internat. Mtg., Soc. Expl. Geophys., Expanded Abstracts, 1711–1714.

Wood, W. T., Stoffa, P. L., and Shipley, T. H., 1994, Quantitative detection of methane hydrate through high-resolution seismic velocity analysis: J. Geophys. Res., **99**, 9681–9695.

Yuan, T., Hyndman, R. D., Spence, G. D., and Desmons, B., 1996, Seismic velocity increase and deep-sea hydrate concentration above a bottom-simulating reflector on the northern Cascadian slope: Jour. Geophys. res., **101**, 13655–13671.